

# Chemical weathering profile in the V–Ti–Fe mine tailings pond: a basalt-weathering analog

Xiaolin Zhang<sup>1,2</sup> · Yinger Deng<sup>1</sup> · Liang Tang<sup>3,4</sup> · Zhengmeng Hou<sup>4</sup> · Jinsong Yang<sup>5</sup>

Received: 8 March 2023 / Revised: 20 July 2023 / Accepted: 5 August 2023 / Published online: 9 September 2023  
© The Author(s), under exclusive licence to Science Press and Institute of Geochemistry, CAS and Springer-Verlag GmbH Germany, part of Springer Nature 2023

**Abstract** The (ultra-)mafic mine tailings pond revealed a weathering discrepancy in the tailings profile, which provided a valuable analog to assess the role of carbonate and silicate weathering of the basalt. In this study, drill-cores samples were selected from the Wanniangou V–Ti–Fe mine tailings pond (Sichuan province, China) to investigate the mineralogic and geochemical characteristics in the tailings profile. The results reveal (1) the tailings pond profile consists of upper and lower layers. The upper layer is composed of carbonate weathering (1.4 %), which was formed in the initial stages of tailings exposure and represented a minimal weathering degree. (2) The lower layer was primarily observed at the aquifer zone of the tailings pond, and was consistent with 0.45 % carbonate weathering and 48.4 % silicate weathering. (3) The weathering discrepancy in the tailings profile could be due to the sulfide oxidation and aerobic/flowing aquifer, which facilitate the water-tailings reactions. The tailings profile provides an analog to studying basalt weathering, as it spans both

carbonate and silicate weathering. This research reinforces the idea that silicate weathering is predominant in basaltic areas and plays a crucial role in regulating atmospheric CO<sub>2</sub> (carbon dioxide) levels on Earth.

**Keywords** V–Ti–Fe mine · Tailings pond profile · Drill core · Basalt weathering

## 1 Introduction

Basalt weathering is a critical factor for regulating atmospheric CO<sub>2</sub> levels on Earth over the long-term carbon cycle, as (ultra-)mafic minerals have a high propensity for weathering and enable net CO<sub>2</sub> fixation (Amiotte Suchet et al. 2003; Dessert et al. 2001, 2003; Li et al. 2022; Taylor and Lasaga 1999; Xiong et al. 2022). Nevertheless, carbonate weathering is also emphasized in basalt weathering (Georg et al. 2007; Jacobson et al. 2015; Nelson et al. 2022). For example, calcite weathering contributes to 0–65 % of the Ca<sup>2+</sup> in non-glacial rivers and 25–90 % of the Ca<sup>2+</sup> in glacial rivers in Iceland (Jacobson et al. 2015). In Deccan Trap basalts of India, roughly 30 % of Ca<sup>2+</sup> is thought to originate from carbonates in basalts and sediments (Das et al. 2005). Nevertheless, the carbonates (or carbonatites) are relatively rare in basalts (Jacobson et al. 2015; Zhang et al. 2023), leading to some debate about their contribution to the overall bulk CO<sub>2</sub> sequestration through chemical weathering. Conversely, the role of carbonate weathering in regulating the global CO<sub>2</sub> balance was highlighted in the Karst area (Dai et al. 2017; Xiao et al. 2023). For example, the carbonate rock chemical weathering of CO<sub>2</sub> sink was 30.3 tons CO<sub>2</sub> km<sup>-2</sup> yr<sup>-1</sup> and 2.43 tons CO<sub>2</sub> km<sup>-2</sup> yr<sup>-1</sup> for silicate weathering in

✉ Yinger Deng  
dengyinge@mail.cduto.edu.cn

<sup>1</sup> College of Environment and Civil Engineering, Chengdu University of Technology, Chengdu, China

<sup>2</sup> Longchang Natural Resources and Planning Bureau, Longchang 642150, Sichuan, China

<sup>3</sup> College of Earth Sciences, Chengdu University of Technology, Chengdu 610059, China

<sup>4</sup> Institute of Subsurface Energy Systems, Clausthal University of Technology, 38678 Clausthal-Zellerfeld, Germany

<sup>5</sup> Key Laboratory of Quaternary Chronology and Hydro-Environmental Evolution, Institute of Hydrogeology and Environmental Geology, China Geological Survey, Shijiazhuang 050061, China

Guizhou province, China (Bai et al. 2023). This inconsistent data suggests that more persuasive evidence is needed to clarify the roles of silicate and carbonate weathering in the basaltic area.

The weathering profile is a unique research objective for understanding the pathway of basalt weathering. Despite extensive research, no sole basalt weathering profile spans the full range of fresh to weathered minerals over geological timescales. Mine tailings are the fine-grained waste of mineral beneficiation, which increases their surface area and allows for faster chemical weathering than uncrushed silicate and carbonate rocks. The (ultra-)mafic tailings pond, therefore, offers a visible profile of fresh and weathered rocks, highlighting the weathering degree discrepancy in the vertical direction. This provides a useful analogue for evaluating the role of silicate and carbonate weathering in basaltic areas. For instance, the weathering rate of tailings can be accelerated by organic/inorganic acids and chelating agents (Schwartzman and Volk 1989). Sulfide oxidation could be a crucial factor in tailings weathering, and the ions flux in the tailings pond are closely correlated with sulfuric acid generation (Zhang et al. 2023). Meanwhile, despite the ions being held in place by the static water table of the tailings pond (Rey et al. 2016), groundwater flow at the bottom of the tailings pond can accelerate weathering and cause weathering discrepancy in the vertical direction (Jackson and Parbhakar-Fox 2016; Wilson et al. 2009).

In this study, the Wanniangou V–Ti–Fe tailings pond in the Panxi region of Sichuan province, China, was selected as the research objective to investigate the weathering profile, assess the contribution of silicate, and carbonate weathering in the ions liberation. The Panxi V–Ti–Fe deposits were linked to the intrusion of Emeishan mafic magma into dolomites of the Neoproterozoic Sinian formations in the Sichuan Basin (Ganino and Arndt 2009; Ganino et al. 2008, 2013; Xing et al. 2012). The Panxi region is known for its abundant deposits of vanadium (V), titanium (Ti), and iron (Fe) ore (Zhou et al. 2005), which have been exploited over the past five decades. Large contact aureoles, mainly composed of brucite marbles, calc-silicate rocks, and skarns, developed at the contact of the intrusions (Ganino et al. 2008). Consequently, calcite was identified in the tailings wastes, and the dissolution was accelerated by sulfide oxidation (sulfuric acid) (Busenberg and Plummer 1982; Davis et al. 2007; Gautelier et al. 1999).

A significant amount of tailings waste has been disposed of in the ponds in the form of slurries due to intensive mining. As of 2021, about 48 tailings ponds had been established and stored roughly 3 billion tons of mine waste, covering 365.6 km<sup>2</sup> of landfills (Tang 2017; Tang et al. 2020, 2021; Tang and Werner 2023). The tailings minerals

include pyroxene, plagioclase, olivine, and amphibole, which have the potential to store anthropogenic CO<sub>2</sub> that is being released into the atmosphere (Berndt et al. 1996; Hangx and Spiers 2009; Meyer et al. 2014; Vogeli et al. 2011). This presents a valuable opportunity to investigate the weathering process, quantify the contributions of silicate and carbonate weathering, and implicate the basalt weathering within a lifelong timescale.

The Wanniangou tailings pond is a typical valley pond, with a designed height of ~ 325 m, and a starter dike designed with a permeable membrane for safety (Table 1). The Wanniangou V–Ti–Fe mine tailings pond is one of the tailings storage facilities for the Pangang Group Company Limited in the Panxi region (Table 1). The storage facility began operating in 2006 and kept running thereafter. In this study, we collected four drill cores samples (Drill-1, Drill-2, Drill-3, and Drill-4) in the pond dam. Our study was conducted with the following objectives in mind: (1) the systematic collection of the drill core samples and the subsequent analysis of mineral and geochemical compositions. (2) We assess the role of silicate and carbonate weathering in the tailings profile. (3) We extended the findings from the (ultra-)mafic tailings weathering to the basalt weathering and emphasized the silicate weathering in the basaltic area.

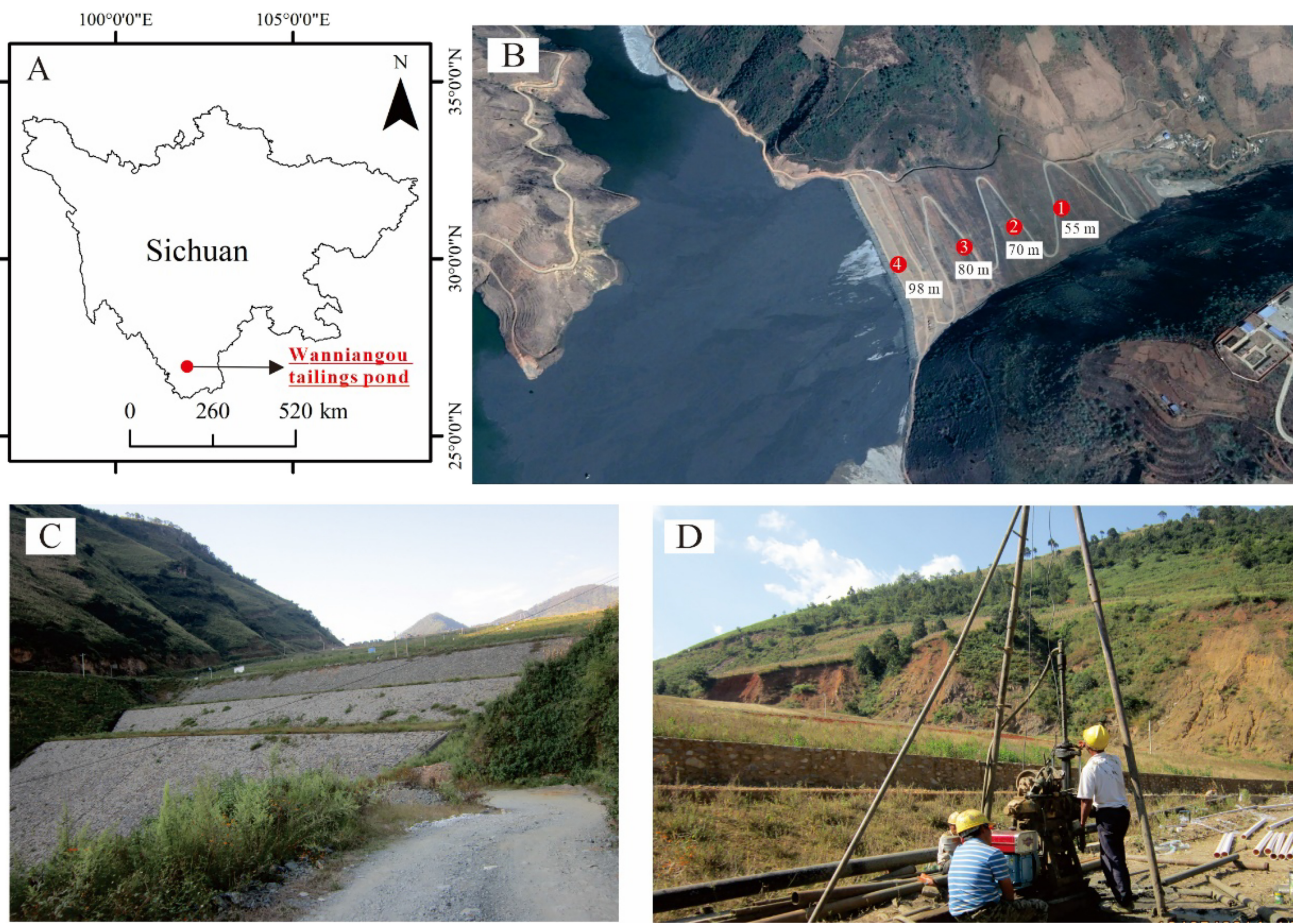
## 2 Research and analytical methods

Four tailings cores were drilled in the tailings dam slope (55, 70, 80, and 98 m long) to identify the chemical weathering profile of the (ultra-)mafic mine tailings (Table 1). The length varies in the drill cores owing to the slope of such hammer-shaped tailings pond. The Drill-1 (shorter core) is near the starter dyke, and the longest core approaches the tailings discharge line (Fig. 1). The core samples along with depths from the surficial slope to the bottom were collected, which is similar to a fine ash tailings dam, in South Africa (Zielke-Olivier and Vermeulen 2019). The shallow tailings layer is relatively chemically stable, with gray and black interlayers, representing unweathered tailings waste, and the samples were collected at 0.5 to 5 m intervals (Fig. 2). Specifically, the sampling of Drill-4 began at 20.7 m since the uniform color and structure in this depth. The colour changes to brown in the deeper layer, and we estimate it might suffer abrupt chemical composition variation. We subsequently collected samples from 0.25 m to 2 m intervals in the lowermost drill cores. Besides, the fresh tailings waste was collected to identify the mineral compositions of the Wanniangou tailings pond (S1 and S2, Table 2).

The samples were dried at 105 °C to eliminate absorbed water prior to conducting spectral measurement. A Mineral

**Table 1** Primary information of Wanniangou tailings pond

Name	Wanniangou tailings pond
Owner	Pangang Group Company Limited, China
Waste type	V-Ti-Fe mine tailings waste (slurry pump)
Start operating	2006
Latitude and longitude	27°07'13" N, 108°8'00" E
Altitude	1395 to 1720 m
Dam height	325 m
Design storage capacity	~0.326 billion m <sup>3</sup>
Reserves	~1.00 billion tons
Designed occupying area	~1.79 km <sup>2</sup>
Pond type	Upstream valley pond
Dam type	Filter rockfill dam
Drill-1	55 m depth
Drill-2	70 m depth
Drill-3	80 m depth
Drill-4	98 m depth

**Fig. 1** Sketch showing the locations of Wanniangou tailings pond. **A** Location of Wanniangou V-Ti-Fe mine tailings pond; **B** remote sensing image of the tailings pond and the drill core sites; **C, D** the field images of the tailings pond

Liberation Analyser (MLA) system was utilized to perform quantitative mineral and material sample analysis, which combined the techniques of Scanning Electron Microscopy

(SEM) and Energy Dispersive X-ray Analysis (EDXA). A Ni standard was utilized to identify minerals with BSE brightness, which were then detected and mapped. The data

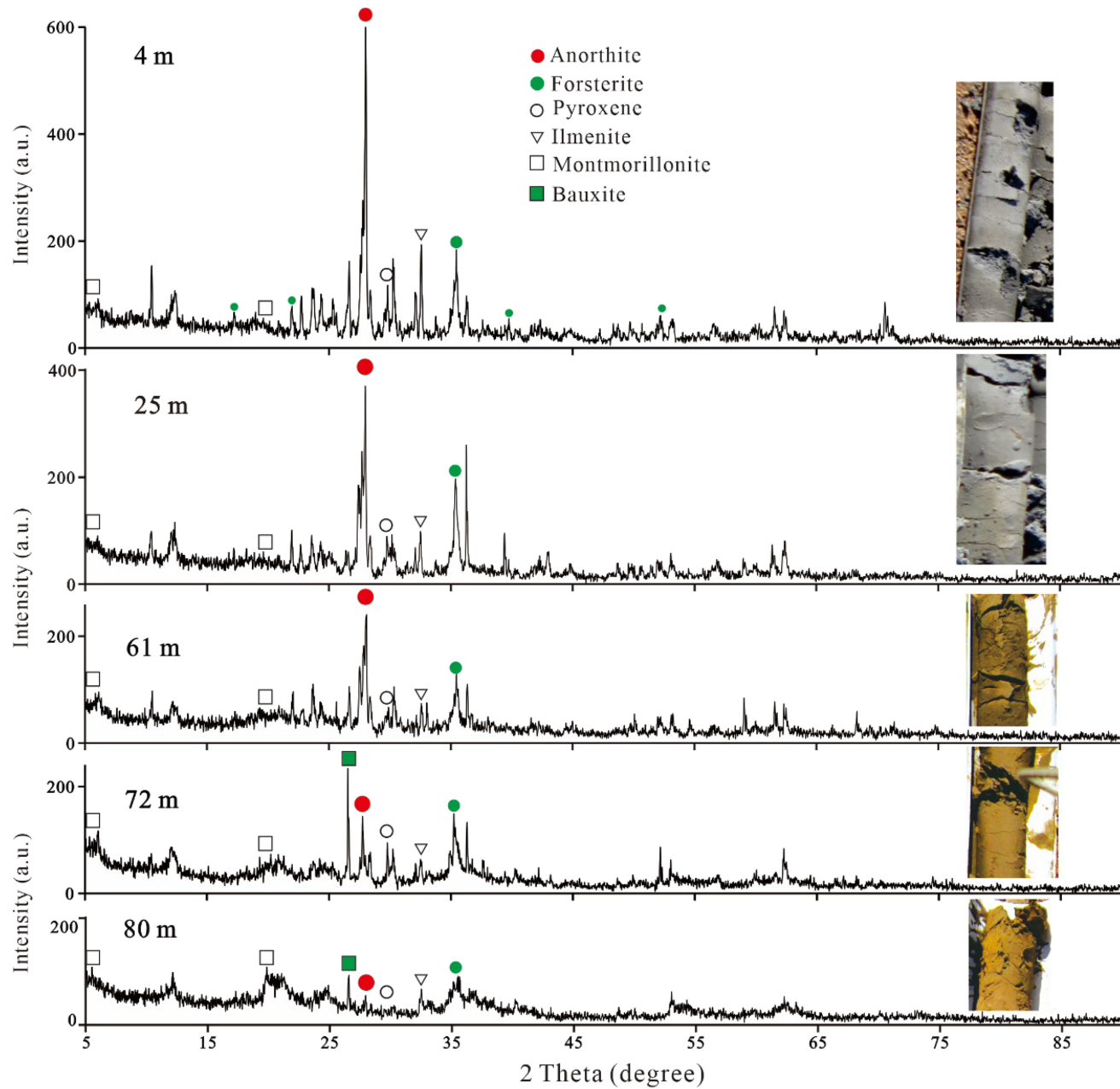


**Fig. 2** Vertical variation of mineral compositions in the tailings pond profile (Drill-3 samples)

were processed using the MLA image viewer to generate classified images based on a site-specific mineral library. The MLA analysis was performed at the State Key Laboratory of Vanadium and Titanium Resources Comprehensive Utilization, China. Besides, an X-Ray Diffractometer (XRD, D8 Advance, Bruker, Germany) was employed to reinforce the mineral compositions and variation in the vertical direction of the tailings pond, Chengdu University of Technology, China. The XRD equipment with Cu K $\alpha$  radiation has a maximum power of 3 kW and a maximum filament voltage of 50 kV, depending on the anode material. The accuracy in peak positions is less than 0.007° 2θ.

The major oxides ( $\text{SiO}_2$ ,  $\text{Al}_2\text{O}_3$ ,  $\text{Fe}_2\text{O}_3$ ,  $\text{MgO}$ ,  $\text{CaO}$ ,  $\text{Na}_2\text{O}$ ,  $\text{K}_2\text{O}$ ,  $\text{MnO}_2$ ,  $\text{P}_2\text{O}_5$  and  $\text{TiO}_2$ ) of the samples were analyzed using an X-Ray Fluorescence spectrometer (XRF, Shimadzu 1800, Japan) at Chengdu University of Technology in China. The XRF analyzer determines the bulk chemical composition with a maximum output power of 4 kW, a maximum current of 140 mA, and a maximum voltage of 60 kV. The analytical precision for major elements was better than 1 %, and detection limits for the major elements were generally better than 30 ppm. In addition, the bulk sulfur and carbon composition (inorganic carbon) of the drill core samples were analyzed using an

**Table 2** The type and abundance of minerals in the fresh waste in the Wanniangou tailings pond

Mineral	S1 (vol.%)	S2 (vol.%)	Arithmetic mean (vol.%)	Standard deviation
Anorthite	38.2	37.9	38.0	0.21
Peridot	12.5	15.5	14.0	2.12
Diopside	10.9	11.0	10.9	0.07
Pyroxene	9.0	7.1	8.0	1.34
Albite	7.9	5.2	6.5	1.91
Chlorite	5.5	6.0	5.7	0.35
Forsterite	4.2	6.3	5.2	1.48
Ilmenite	3.9	3.3	3.6	0.42
Orthoclase	2.4	1.6	2.0	0.57
Biotite	1.4	1.6	1.5	0.14
Quartz	1.3	1.1	1.2	0.14
Magnetite	0.69	0.69	0.69	0.00
Pyrrhotite	0.53	0.67	0.60	0.10
Fayalite	0.32	0.33	0.33	0.01
Calcite	0.15	0.19	0.17	0.03
Apatite	0.13	0.13	0.13	0.00
Calcium ferrite	0.1	0.08	0.09	0.01
Chalcopyrite	0.02	0.05	0.04	0.02

Elemental Analyzer (EA, Rapid CS cube, Elementar, German) at the Institute of Hydrogeology and Environmental Geology (IHEG), Chinese Academy of Geological Sciences (CAGS), Shijiazhuang, China. The elemental analyzer can quickly measure total carbon content, with an RSD of less than 1% for repeated measurements. The measurement ranges from 0–100 % or 0.01–40 mg absolute carbon contents.

### 3 Results

#### 3.1 Mineralogy

Table 2 displays the mineral composition of the Wanniangou V–Ti–Fe mine tailings pond, with anorthite being the most abundant mineral (37.9 to 38.2 vol. %). Other minerals include peridot (12.5 to 15.5 vol.%) > diopside (10.9 to 11.0 vol.%) > pyroxene (7.1 to 9.0 vol.%) > albite (5.2 to 7.9 vol.%) > chlorite (5.5 to 6.0 vol.%) > forsterite (4.2 to 6.3 vol.%) > ilmenite (3.3 to 3.9 vol.%) > orthoclase (1.6 to 2.4 vol.%) > biotite (1.4 to 1.6 vol.%) > quartz (1.1 to 1.3 vol.%). The presence of sulfide minerals, such as pyrrhotite and chalcopyrite, is at a lesser level. Likewise, the levels of calcite and apatite are minor, accounting for 0.15 to 0.19 vol.% and 0 to 0.13 vol.%, respectively. Generally, the sulfide oxidation in the tailings can generate sulfuric acid ( $H_2SO_4$ ), which can be

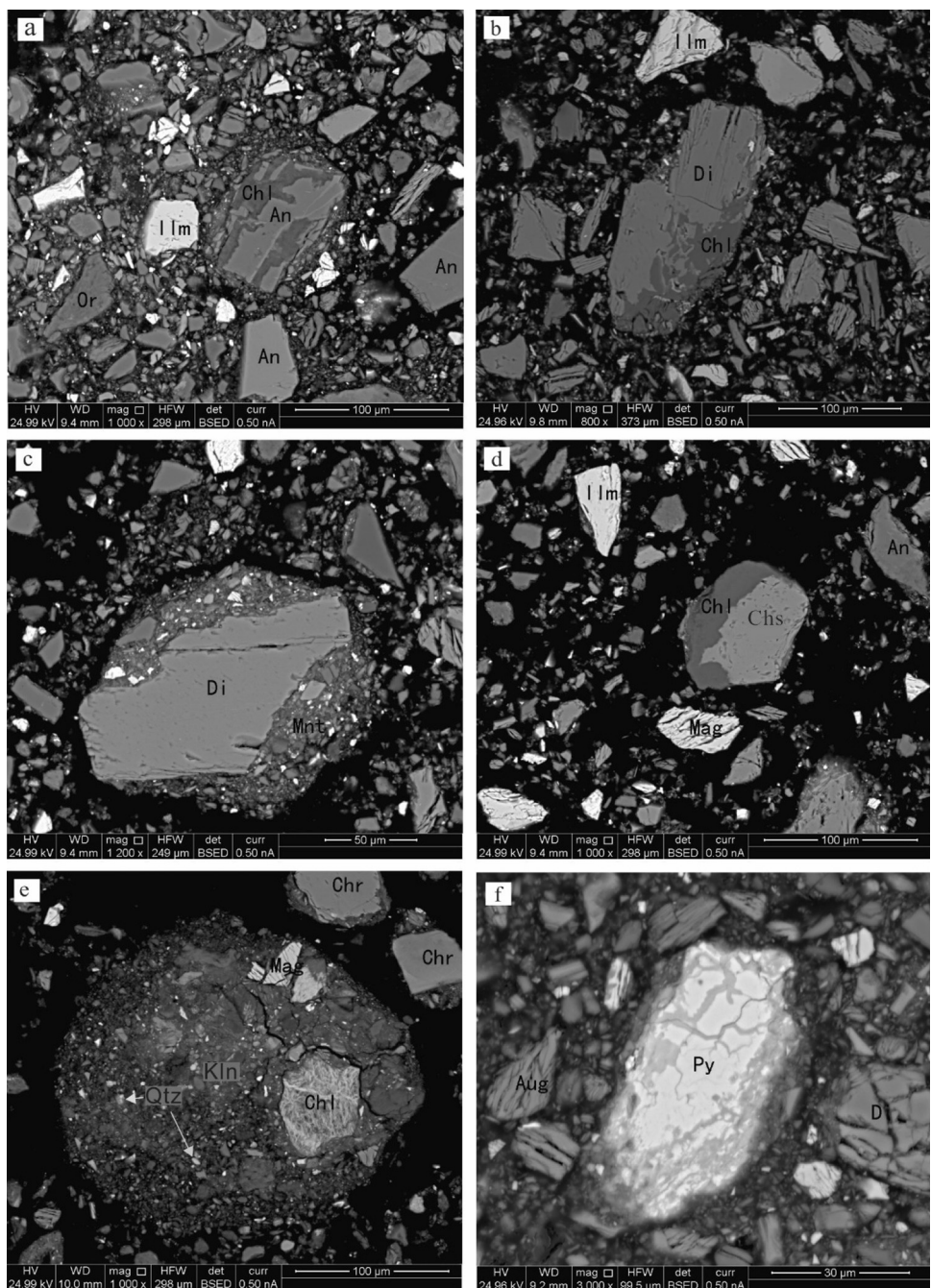
neutralized by calcite and dolomite (Tang 2017; Xu et al. 2022; Zhang et al. 2023).

In Fig. 2, the mantle-derived minerals (e.g., anorthite, forsterite, and pyroxene) are subject to intensify chemical weathering, leading to a decrease (both in mineral and chemical contents) in the vertical direction and nearly depletion at the bottom of the tailings profile. In comparison, the secondary efflorescent phases (e.g., kaolinite, montmorillonite, and bauxite) emerge in the deeper tailings pond. The decomposition of minerals is visible in the SEM images presented in Fig. 3. For instance: (1) the efflorescent phases exhibit semi-euhedral crystal clusters. (2) The anorthite erodes have been transformed into chlorite, with the edges of the diopside being weathered into chlorite. The chrysotile experiences a similar transformation in mineral decomposition. (3) The diopside and chlorite altered into kaolinite or montmorillonite. (4) The pyrite particles are irregular in shape, and the residues were weathered.

#### 3.2 Vertical geochemical discrepancy

In Table 3, the bulk elements present in the tailings pond are  $SiO_2$  (26.52 to 43.84, mean 37.25 wt.%),  $Fe_2O_3$  (15.22 to 32.06, mean 22.29 wt.%),  $Al_2O_3$  (8.86 to 21.2, mean 12.45 wt.%),  $MgO$  (2.45 to 16.2, mean 11.85 wt.%),  $CaO$  (0.93 to 7.78, mean 5.03 wt.%),  $TiO_2$  (2.98 to 7.01, mean 4.56 wt.%), and  $Na_2O$  (0.37 to 2.23, mean 1.40 wt.%). The tailings are predominantly composed of inorganic carbon,

**Fig. 3** Primary and secondary minerals in the tailings profile. The SEM images were captured from Drill-1. (An: Anorthite; Aug: Augite; Chl: Chlorite; Di: Diopside; Or: Orthoclase; Ilm: Ilmenite; Mag: Magnetite; Chs: Chrysotile; Qtz: Quartz; Py: Pyrite; Mnt: Montmorillonite; Chr: Chromite; Kln: Kaolinite)



with organic carbon being negligible. This is because of the toxic substances in the tailings that inhibit plant growth. Meanwhile, the vanadium-titanium magnetite is dressed using gravity and magnetic separation without any organic flotation (Tang 2017). The minor elements identified include SO<sub>3</sub> (0.05 to 1.32, mean 0.61 wt.%), K<sub>2</sub>O (0.23 to 1.019, mean 0.48 wt.%), MnO (0.205 to 0.34, mean 0.26 wt.%), P<sub>2</sub>O<sub>5</sub> (0.07 to 0.188, mean 0.12 wt.%), V<sub>2</sub>O<sub>5</sub> (0.035 to 0.176, mean 0.08 wt.%), inorganic carbon (0 to 0.177, mean 0.04 wt.%), BaO (0.025 to 0.068, mean 0.04 wt.%), and Cr<sub>2</sub>O<sub>3</sub> (0.002 to 0.0177, mean 0.01 wt.%).

### 3.2.1 Soluble elements

The tailings pond profile exhibits a heterogeneous distribution of chemical dissolution along with depth. Figure 4 depicts the decline of CaO, MgO, Na<sub>2</sub>O, and SO<sub>3</sub> in the tailings pond profile, and the Al<sub>2</sub>O<sub>3</sub>, BaO, and P<sub>2</sub>O<sub>5</sub> are slightly enriched in the bottom. On the other hand, the SiO<sub>2</sub>, Cr<sub>2</sub>O<sub>3</sub>, TiO<sub>2</sub>, V<sub>2</sub>O<sub>5</sub>, K<sub>2</sub>O, Fe<sub>2</sub>O<sub>3</sub>, MnO, and inorganic carbon keep constant in the profile. Besides, the correlation coefficient (*r*) is used to assess the relationship between two variables (Taylor 1990). It affirms that *r* less than 0.1

**Table 3** Geochemical composition and Chemical Index of Alteration (CIA) of drill cores in Wanniangou tailings pond profile

	Depth (m)	SiO <sub>2</sub> (wt.%)	Al <sub>2</sub> O <sub>3</sub>	Fe <sub>2</sub> O <sub>3</sub>	MgO	CaO	Na <sub>2</sub> O	K <sub>2</sub> O	MnO	TiO <sub>2</sub>	V <sub>2</sub> O <sub>5</sub>	Cr <sub>2</sub> O <sub>3</sub>	BaO	SO <sub>3</sub>	P <sub>2</sub> O <sub>5</sub>	Inorganic Carbon	CIA
Drill-1	1.5	33.40	9.00	27.28	14.39	5.95	1.19	0.253	0.305	6.86	0.122	0.002	0.031	1.065	0.085	0.018	41
	4	35.43	10.68	24.89	13.06	5.53	1.33	0.400	0.272	5.80	0.109	0.008	0.035	0.748	0.100	0.030	46
	10	33.72	9.25	28.07	13.16	5.23	1.29	0.440	0.282	5.91	0.144	0.011	0.028	0.827	0.088	0.020	44
	14	35.89	10.04	25.75	13.23	5.42	1.48	0.529	0.279	5.95	0.116	0.007	0.037	0.880	0.099	0.023	44
	16	34.64	9.50	26.18	12.48	5.62	1.38	0.448	0.287	6.60	0.120	0.007	0.036	0.748	0.113	0.015	43
	25	32.36	9.54	28.87	12.15	5.63	1.23	0.346	0.295	6.78	0.151	0.007	0.029	0.712	0.101	0.040	44
	27	38.75	11.68	22.93	10.36	5.85	1.87	0.701	0.236	4.01	0.112	0.008	0.042	0.399	0.129	0.022	45
	32	38.32	12.10	20.20	12.77	5.36	1.35	0.363	0.247	4.03	0.059	0.004	0.038	0.479	0.145	0.010	50
	34	37.66	12.38	23.11	11.06	5.54	1.58	0.498	0.235	3.88	0.107	0.008	0.038	0.405	0.114	0.034	49
	38	39.50	12.04	19.41	13.67	5.56	1.54	0.429	0.246	4.05	0.049	0.002	0.034	0.580	0.130	0.019	48
Drill-2	39	38.10	11.59	22.01	12.56	4.82	1.80	0.546	0.244	4.10	0.081	0.006	0.034	0.567	0.116	0.023	49
	43	39.99	11.74	18.98	13.54	5.10	1.54	0.603	0.235	3.76	0.050	0.004	0.037	0.756	0.135	0.016	49
	50	37.87	12.44	21.90	11.88	4.48	1.32	0.462	0.258	4.27	0.069	0.003	0.039	0.356	0.124	0.022	54
	53	33.85	17.52	25.17	7.05	2.72	0.78	0.355	0.287	4.68	0.067	0.004	0.046	0.106	0.125	0.059	74
	55	33.46	20.23	23.08	5.52	1.64	0.54	0.299	0.289	3.87	0.049	0.004	0.054	0.073	0.122	0.054	85
	57	37.06	10.13	23.29	13.76	5.87	1.53	0.52	0.28	5.94	0.086	0.0023	0.033	0.96	0.11	0.021	43
	7.7	34.46	10.39	25.21	12.21	6.29	1.36	0.36	0.28	6.42	0.114	0.0076	0.034	0.88	0.10	0.102	44
	10	36.98	9.95	22.56	15.60	5.75	1.36	0.39	0.27	5.29	0.075	0.0029	0.031	0.99	0.09	0.052	44
	20.7	37.07	10.80	24.27	12.30	5.90	1.59	0.55	0.25	4.84	0.117	0.0079	0.036	0.72	0.11	0.041	44
	27	39.98	11.45	18.99	14.76	6.38	1.56	0.41	0.23	3.55	0.059	0.0044	0.035	0.78	0.11	0.052	45
Drill-3	33	39.19	11.21	20.10	13.88	5.93	1.61	0.53	0.24	4.02	0.072	0.0034	0.036	0.83	0.09	0.082	46
	46	38.38	11.20	20.57	13.84	4.92	1.34	0.46	0.25	4.01	0.057	0.0041	0.038	0.71	0.12	0.031	50
	50	38.98	11.88	19.58	13.88	5.10	1.43	0.41	0.24	3.90	0.054	0.0049	0.040	0.58	0.14	0.012	50
	55	39.44	11.92	19.03	13.22	5.39	1.50	0.55	0.24	3.93	0.053	0.0034	0.037	0.75	0.13	0.026	49
	61	38.21	10.93	21.71	13.25	4.98	1.40	0.63	0.25	4.34	0.082	0.0059	0.037	0.69	0.11	0.051	49
	63	39.05	11.40	20.33	14.12	5.07	1.48	0.53	0.25	4.17	0.063	0.0041	0.038	0.76	0.11	0.023	49
	64	38.11	12.11	22.46	11.37	4.68	1.33	0.57	0.27	4.87	0.078	0.0037	0.038	0.30	0.12	0.061	53
	65	35.99	12.14	24.67	10.35	4.14	1.21	0.62	0.29	5.28	0.093	0.0043	0.034	0.28	0.12	0.052	56
	68	33.00	15.91	25.78	7.86	2.61	0.79	0.34	0.29	5.38	0.089	0.0044	0.048	0.11	0.12	0.021	72
	70	26.52	18.51	32.06	3.10	0.93	0.37	0.23	0.34	6.20	0.113	0.0029	0.047	0.05	0.14	0.148	94
Drill-3	4	39.42	12.47	19.24	12.06	6.81	1.78	0.57	0.25	5.25	0.052	0.0060	0.038	1.32	0.11	0.031	44
	7	38.30	10.91	21.54	12.16	6.26	1.63	0.61	0.26	5.27	0.081	0.0049	0.036	0.92	0.10	0.046	43
Drill-3	12.2	40.67	11.64	18.37	13.97	6.38	1.73	0.55	0.23	3.62	0.053	0.0024	0.033	0.75	0.09	0.021	44
	20	29.95	8.86	31.41	12.76	4.80	1.18	0.29	0.30	7.01	0.175	0.0093	0.028	0.87	0.07	0.025	45

Table 3 continued

	Depth (m)	SiO <sub>2</sub> (wt %)	Al <sub>2</sub> O <sub>3</sub>	Fe <sub>2</sub> O <sub>3</sub>	MgO	CaO	Na <sub>2</sub> O	K <sub>2</sub> O	MnO	TiO <sub>2</sub>	V <sub>2</sub> O <sub>5</sub>	Cr <sub>2</sub> O <sub>3</sub>	BaO	SO <sub>3</sub>	P <sub>2</sub> O <sub>5</sub>	Inorganic Carbon	CIA
	25	34.87	10.33	27.07	12.32	5.30	1.45	0.57	0.26	4.94	0.147	0.0095	0.031	0.79	0.08	0.020	45
	34	30.30	8.88	31.05	12.76	5.22	1.11	0.24	0.29	6.35	0.176	0.0177	0.025	0.84	0.09	0.030	44
49	34.22	10.41	27.45	12.40	5.13	1.42	0.36	0.28	5.46	0.137	0.0065	0.032	0.65	0.11	0.025	47	
53	37.23	11.57	23.32	12.19	5.39	1.51	0.42	0.26	4.92	0.094	0.0088	0.033	0.44	0.11	0.016	48	
61	40.24	11.98	19.45	12.36	5.90	1.71	0.55	0.24	3.95	0.063	0.0056	0.036	0.61	0.13	0.024	46	
64	39.07	11.68	20.92	13.37	5.29	1.43	0.46	0.25	4.14	0.063	0.0039	0.040	0.53	0.12	0.024	49	
70	36.31	13.30	22.13	10.83	4.23	1.11	0.32	0.27	4.30	0.054	0.0027	0.046	0.18	0.12	0.030	58	
72	34.18	14.26	25.68	9.29	3.30	0.94	0.43	0.30	5.19	0.084	0.0067	0.046	0.26	0.13	0.062	66	
78	32.09	21.06	24.56	4.36	1.41	0.60	0.41	0.24	3.94	0.067	0.0065	0.052	0.14	0.15	0.177	90	
80	31.30	21.20	26.03	3.45	1.03	0.41	0.35	0.28	4.09	0.067	0.0048	0.056	0.08	0.14	0.125	92	
Drill 4	20.7	43.84	14.47	15.22	10.56	7.78	2.23	0.667	0.205	3.48	0.041	0.003	0.039	0.786	0.125	0.030	44
	27	42.20	13.24	16.05	13.48	6.49	1.95	0.543	0.208	2.98	0.035	0.004	0.038	0.833	0.101	0.054	47
	33.8	42.14	13.08	17.89	11.97	6.69	2.02	0.701	0.218	3.50	0.061	0.004	0.038	0.751	0.108	0.046	45
	40	42.46	13.63	16.72	13.02	6.53	1.94	0.551	0.215	3.44	0.043	0.004	0.037	0.756	0.107	0.051	47
47	40.74	11.64	17.06	15.40	5.66	1.58	0.547	0.226	3.51	0.037	0.006	0.033	1.001	0.113	0.048	47	
54.6	42.27	12.19	16.98	13.98	6.08	1.74	0.520	0.221	3.24	0.042	0.003	0.036	0.709	0.116	0.070	47	
61	39.05	11.34	18.52	15.11	5.73	1.46	0.305	0.227	3.35	0.048	0.006	0.033	0.845	0.122	0.017	47	
67.7	39.13	10.45	18.37	16.20	5.20	1.42	0.461	0.24	3.77	0.042	0.002	0.032	1.014	0.116	0.031	47	
72	39.41	10.69	18.38	15.82	5.18	1.42	0.478	0.233	3.72	0.046	0.002	0.038	0.977	0.114	0.042	47	
77	39.44	12.04	18.67	14.05	5.94	1.57	0.402	0.216	3.37	0.064	0.004	0.039	0.719	0.109	0.047	47	
84	38.86	12.29	20.30	12.19	6.06	1.58	0.364	0.245	4.09	0.066	0.004	0.036	0.516	0.127	0.000	47	
86	38.20	11.89	21.73	11.91	6.13	1.64	0.402	0.25	4.57	0.085	0.004	0.039	0.556	0.127	0.058	46	
90	39.14	13.47	20.53	10.72	4.71	1.42	0.532	0.25	3.82	0.059	0.004	0.042	0.373	0.129	0.059	55	
92	39.20	13.82	20.83	9.78	3.45	1.17	0.800	0.261	3.93	0.058	0.003	0.049	0.230	0.135	0.059	62	
96	39.13	13.89	20.76	10.00	3.53	1.21	0.760	0.259	4.06	0.058	0.003	0.044	0.247	0.135	0.000	60	
98	36.18	20.38	22.51	2.45	1.56	1.43	1.019	0.255	3.74	0.063	0.006	0.068	0.066	0.188	0.136	80	

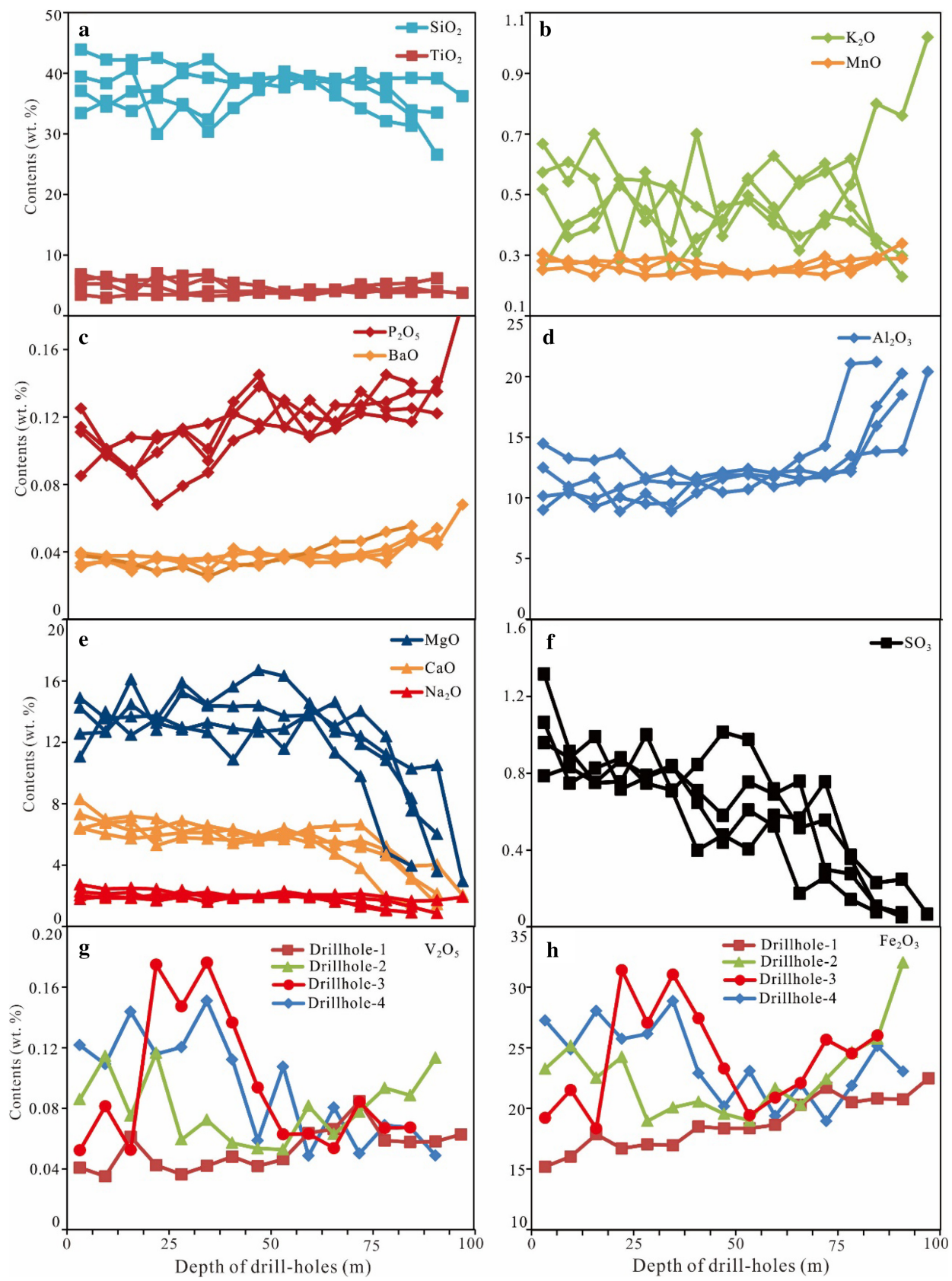


**Fig. 4** Chemical compositions characteristic in the tailings profile

indicates a negligible relationship, while a value greater than 0.9 signifies a very strong relationship; values in-between are subject to disputable (Schober et al. 2018). For example, the  $r$  equivalent to 0.42 suggests that  $\sim 18\%$  of the variability can be explained (Nishimura et al. 2016). In Table 4, the geochemistry of the tailings pond profile exhibits a negative correlation with depth (m), the  $r$  less than -0.1 for the elements  $\text{SO}_3$ ,  $\text{CaO}$ ,  $\text{Na}_2\text{O}$ ,  $\text{MgO}$ ,  $\text{SiO}_2$ ,  $\text{Cr}_2\text{O}_3$ ,  $\text{TiO}_2$ , and  $\text{V}_2\text{O}_5$ . This suggests these elements are likely to dissolve. Meanwhile, the  $r$  larger than -0.1 represents the elements that are stabilizing in the profile (e.g.,  $\text{Fe}_2\text{O}_3$ ,  $\text{MnO}$ , inorganic carbon,  $\text{Al}_2\text{O}_3$ ,  $\text{BaO}$ , and  $\text{P}_2\text{O}_5$ ). However, this conclusion should be used judiciously because (1) when the  $r$  cutoff points range from -0.26 to 0.28 (including  $\text{SiO}_2$ ,  $\text{Cr}_2\text{O}_3$ ,  $\text{TiO}_2$ ,  $\text{V}_2\text{O}_5$ ,  $\text{K}_2\text{O}$ ,  $\text{Fe}_2\text{O}_3$ ,  $\text{MnO}$ , and inorganic carbon), the standard deviation is greater than  $r$ , demonstrating the geochemical features in the profile are complex in the vertical direction, that is not necessarily correlated with depth. (2) In the case of  $-0.26 \leq r \leq 0.28$ , the majority of the confidence intervals (two-tailed) are less than 95%, indicating low confidence in the correlation. (3) Generally, the  $\text{TiO}_2$ ,  $\text{V}_2\text{O}_5$ ,  $\text{K}_2\text{O}$ , and  $\text{Fe}_2\text{O}_3$  are relatively stable in the surficial environment (Shi et al. 2020a, b).

On this basis, we divided the geochemical elements of the tailings profile into three elements categories, i.e. the soluble element ( $\text{SO}_3$ ,  $\text{CaO}$ ,  $\text{Na}_2\text{O}$ , and  $\text{MgO}$ ), semi-transfer element ( $\text{Al}_2\text{O}_3$ ,  $\text{BaO}$ , and  $\text{P}_2\text{O}_5$ ) and constant elements ( $\text{SiO}_2$ ,  $\text{Cr}_2\text{O}_3$ ,  $\text{TiO}_2$ ,  $\text{V}_2\text{O}_5$ ,  $\text{K}_2\text{O}$ ,  $\text{Fe}_2\text{O}_3$ ,  $\text{MnO}$ , inorganic carbon, Table 4). The calcite in tailings could

preferentially dissolve in groundwater, leading to a more rapid descent in  $\text{CaO}$  concentration. In Fig. 4, the soluble elements ( $\text{SO}_3$ ,  $\text{CaO}$ ,  $\text{Na}_2\text{O}$ , and  $\text{MgO}$ ) are declining in the profile, which is consistent with the strongest negative correlation. Similarly, the  $r$  between depth and  $\text{CaO}$ , and  $\text{MgO}$  are also negative at -0.74 and -0.55, respectively. The Panxi V-Ti-Fe deposits were linked to the intrusion of Emeishan mafic magma into dolomites of the Neoproterozoic Sinian formations in the Sichuan Basin (Ganino and Arndt 2009; Ganino et al. 2008, 2013; Xing et al. 2012). Large contact aureoles, mainly composed of brucite marbles, calc-silicate rocks, and skarns, developed at the contact of the intrusions (Ganino et al. 2008). Consequently, calcite was identified in the tailings wastes (mean 0.17 vol.%, Table 2), and the dissolution is directly proportional to  $\text{H}^+$  activity (Busenberg and Plummer 1982; Davis et al. 2007; Gautier et al. 1999).

Meanwhile, the negative correlation between depth and  $\text{Na}_2\text{O}$  ( $r$ : -0.58) suggests that Na-silicate is soluble in the tailings profile. The V-Ti-Fe ore was separated using gravity and magnetic separation methods without the addition of Na-enriched chemical agents (Tang 2017). Consequently, the variation of  $\text{Na}_2\text{O}$  observed in the tailings profile could depend fairly on mineral degeneration. Normally, Na occurs in the diopside (mean 10.9 vol.%) and albite (6.5 vol.%). In Fig. 2, the diopside is actively involved in the water-tailings reaction and minimized to zero with depth, while the albite is relatively stable. Therefore, silicate weathering, particularly diopside, in the

**Table 4** Pearson correlation coefficient ( $r$ ) between geochemical of tailings and depth in the Wanniangou tailings pond

Elements categories	Elements	Average ( $r$ )	Standard deviation	Drill-1 ( $r$ )	Drill-2 ( $r$ )	Drill-3 ( $r$ )	Drill-4 ( $r$ )
Soluble elements	$\text{SO}_3$	-0.81	0.08	-0.84**	-0.79**	-0.92**	-0.69**
	$\text{CaO}$	-0.74	0.03	-0.70**	-0.71**	-0.76**	-0.78**
	$\text{Na}_2\text{O}$	-0.58	0.22	-0.27	-0.52*	-0.68**	-0.87**
	$\text{MgO}$	-0.55	0.10	-0.64*	-0.53*	-0.64*	-0.40
Semi-transfer elements	$\text{Al}_2\text{O}_3$	0.57	0.22	0.78**	0.64**	0.64*	0.21
	$\text{BaO}$	0.64	0.08	0.67**	0.69**	0.69**	0.50*
	$\text{P}_2\text{O}_5$	0.70	0.07	0.73**	0.63*	0.80**	0.60*
Constant elements	$\text{SiO}_2$	-0.26	0.43	0.33	-0.22	-0.27	-0.90**
	$\text{Cr}_2\text{O}_3$	-0.20	0.17	-0.46	-0.17	-0.17	0.00
	$\text{TiO}_2$	-0.18	0.54	-0.77**	-0.22	-0.44	0.70**
	$\text{V}_2\text{O}_5$	-0.14	0.51	-0.77**	-0.16	-0.28	0.66**
	$\text{K}_2\text{O}$	-0.03	0.24	0.09	0.09	-0.43	0.15
	$\text{Fe}_2\text{O}_3$	0.14	0.54	-0.60*	0.15	0.08	0.93**
	$\text{MnO}$	0.22	0.45	-0.36	0.21	0.13	0.91**
	Inorganic carbon	0.28	0.21	0.45	0.02	0.52	0.14

(1)\*\* 99% confidence interval (two-tailed). \* 95% confidence interval (two-tailed)

(2) The average correlation is the arithmetic mean of four drill cores

tailings profile could play a role in regulating the Na migration in the tailings profile.

### 3.2.2 Semi-transfer elements

The semi-transfer elements, including  $\text{Al}_2\text{O}_3$ ,  $\text{BaO}$ , and  $\text{P}_2\text{O}_5$ , are present in the tailings. The presence of Al is observed to be abundant in the basalt minerals, consistent with pyroxene and plagioclase (Tang 2017). However, these minerals are susceptible to migration in supergene environments (Velbel and Barker 2008). For instance, the montmorillonite formed around the diopside and was accompanied by tiny, irregularly shaped chlorite (Fig. 3). Meanwhile, due to the sulfide oxidation, the presence of  $\text{H}_2\text{SO}_4$  (pH: 4.7 to 5.2) can lead to incomplete neutralization by the dissolution of aluminum phases (Johnson et al. 1981). In a neutral environment, the Al,  $\text{BaO}$ , and  $\text{P}_2\text{O}_5$  can jointly form colloids and precipitate in the tailings pond. As a result, there is a slight enrichment in the concentration of  $\text{Al}_2\text{O}_3$ ,  $\text{BaO}$ , and  $\text{P}_2\text{O}_5$  in the tailings profile (Fig. 4), and the correlation with depth is 0.57, 0.64, and 0.70, respectively (Table 4).

### 3.2.3 Constant elements

Generally, Al and Fe exhibit similar geochemical properties in the weathering profile of basalt (Liu et al. 2021). Nevertheless, the Wanniangou tailings profile reveals a discrepancy between Al and Fe. The Al is collectively enriched at the bottom; while Fe depicts greater diversity in the tailings profile ( $r$  varies from -0.60 to 0.93, Table 4). In Fig. 5,  $\text{Fe}_2\text{O}_3$  shows a negative correlation with  $\text{SiO}_2$  ( $r$ : -0.945), but positive correlations with  $\text{V}_2\text{O}_5$  ( $r$ : 0.878) and  $\text{TiO}_2$  ( $r$ : 0.843). This evidence suggests that a higher proportion of  $\text{Fe}_2\text{O}_3$ ,  $\text{V}_2\text{O}_5$ , and  $\text{TiO}_2$  are derived from the same sources. The Fe originates mainly from pyroxene, ilmenite, and titanomagnetite in the V-Ti-Fe mine tailings (Tang 2017). The pyroxene is active in the surficial environment; conversely, the ilmenite and titanomagnetite are stable (Hill et al. 2000; Yamada and Shoji 1987; Yang 1987). First, the  $\text{V}_2\text{O}_5$  is isomorphism with vanadium titanium magnetite minerals, such as maghemite, bixbyite, and vanadium oxide (Li et al. 2021). Second, the  $\text{TiO}_2$  remains fairly constant in the vertical direction and is associated with ilmenite and magnetite. Therefore, the fluctuations in  $\text{V}_2\text{O}_5$  and  $\text{TiO}_2$  could connect to the iron levels in the tailings profile.

The potassium is initially derived from silicate weathering (Dansgaard 1964). In Table 2, potassium exists in the forms of orthoclase (mean 2.01 vol.%) and biotite (mean 1.49 vol.%). These minerals are very stable in the surficial environment and consequently characteristics a very weak correlation with depth ( $r$ : 0.03, Table 4). The average

inorganic carbon of the V-Ti-Fe mine tailings pond in the Panxi region was  $0.10 \pm 0.10$  wt.% (based on 48 tailings ponds, Appendix data) (Tang 2017). The tailings profile is slightly lower in carbon contents, ranging from 0 to 0.18 wt.% (mean 0.04 wt.%). Besides, the variation in carbon is weakly correlated with depth ( $r$ : 0.28), and the carbon contents are not significantly decreased in the profile, this evidence indicating an equilibrium between the dissolution and precipitation of carbonate (Fig. 4).

### 3.3 Weathering degree in the profile

The Chemical Index of Alteration (CIA) was initially introduced as a tool to monitor the decomposition of unstable minerals (Nesbitt and Young 1982):

$$\text{CIA} = 100 \times \frac{\text{Al}_2\text{O}_3}{\text{Al}_2\text{O}_3 + \text{CaO}^* + \text{Na}_2\text{O} + \text{K}_2\text{O}} \quad (1)$$

The CIA reflects the degree of weathering by measuring the dissolution of feldspar and clay minerals in the tailings profile. In Eq. 1, the  $\text{CaO}$  represents the silicate fraction, which corrects the  $\text{CaO}$  content from the presence of carbonates (e.g., calcite, dolomite) and phosphates (e.g., apatite) (McLennan 1993). The  $\text{CaO}$  (silicate fraction) in the tailings profile can be considered equal to the bulk  $\text{CaO}$ , corrected for carbonates and phosphates, as it contains inorganic carbon (mean 0.04 wt.%) and  $\text{P}_2\text{O}_5$  (mean 0.12 wt.%). As a result, the Wanniangou tailings pond profile shows a significant variation of CIA from 41 to 94 (Drill-1: 41–85, Drill-2: 43–94, Drill-3: 43–92, Drill-4: 44–80, Table 3). The CIA keeps in equilibrium at the shallow zone but increases sharply at the deeper zone of the tailings pond, which is assumed to relate to aquifer-induced water-tailings reaction.

### 3.4 Horizontal homogenous of tailings profile

The diversity in spatial weathering regarding tailings ponds is closely connected with depth, alternatively reflecting the duration of weathering and the hydrogeochemistry conditions of tailings ponds. For example, the Wanniangou tailings pond was established in 2006 and expanded both horizontally and vertically in subsequent years (Table 1). This resulted in the deposition of mine waste at different heights at different times, with older waste deposited at the bottom and the fresher slurry dumped on the surficial beach. This is reflected in the drill cores, where the lower altitude embankment (Drill-1) is thought to represent the historically weathered tailings waste. Meanwhile, the higher workbench (Drill-4) represents the fresh or less weathered mine tailings.

However, the shallow layers of the drill cores (Drill-1  $\leq \sim 50$  m; Drill-2 and Drill-3  $\leq \sim 64$  m; Drill-

	SiO <sub>2</sub>	Al <sub>2</sub> O <sub>3</sub>	Fe <sub>2</sub> O <sub>3</sub>	MgO	CaO	Na <sub>2</sub> O	K <sub>2</sub> O	MnO	TiO <sub>2</sub>	V <sub>2</sub> O <sub>5</sub>	Cr <sub>2</sub> O <sub>3</sub>	BaO	SO <sub>3</sub>	P <sub>2</sub> O <sub>5</sub>	Carbon
SiO <sub>2</sub>	1														
Al <sub>2</sub> O <sub>3</sub>	-0.21	1													
Fe <sub>2</sub> O <sub>3</sub>	-0.95	-0.01	1												
MgO	0.52	-0.88	-0.39	1											
CaO	0.62	-0.77	-0.44	0.82	1										
Na <sub>2</sub> O	0.81	-0.52	-0.64	0.62	0.87	1									
K <sub>2</sub> O	0.55	0.11	-0.44	-0.08	0.09	0.49	1								
MnO	-0.89	0.07	0.89	-0.41	-0.53	-0.74	-0.46	1							
TiO <sub>2</sub>	-0.74	-0.34	0.84	-0.05	-0.06	-0.36	-0.41	0.84	1						
V <sub>2</sub> O <sub>5</sub>	-0.71	-0.38	0.88	-0.05	-0.02	-0.23	-0.32	0.64	0.83	1					
Cr <sub>2</sub> O <sub>3</sub>	-0.46	-0.25	0.58	-0.04	0.02	-0.09	-0.17	0.28	0.47	0.74	1				
BaO	-0.13	0.89	-0.05	-0.82	-0.74	-0.45	0.30	0.07	-0.33	-0.38	-0.28	1			
SO <sub>3</sub>	0.33	-0.75	-0.23	0.81	0.79	0.59	-0.04	-0.29	0.16	0.09	0.11	-0.74	1		
P <sub>2</sub> O <sub>5</sub>	0.11	0.67	-0.26	-0.57	-0.51	-0.19	0.35	-0.13	-0.46	-0.51	-0.34	0.75	-0.63	1	
Carbon	-0.35	0.67	0.18	-0.65	-0.56	-0.44	0.05	0.16	-0.05	-0.07	-0.05	0.58	-0.39	0.36	1

**Fig. 5** Pearson correlation coefficient of geochemical elements in the tailings profile

$4 \leq \sim 90$  m) are quite geochemical homogeneous (Fig. 4). Because (1) the grayish color in the shallow tailings indicates that the waste has not undergone much chemical weathering (Fig. 2). (2) The low coefficient variation in the upper layer of Al<sub>2</sub>O<sub>3</sub> (9.9), MgO (8.5), and CaO (9.6) disclose the shallow profiles collectively endure less variation. However, in the deeper zone, the coefficient variation of Al<sub>2</sub>O<sub>3</sub>, MgO, and CaO are elevated to 23.9, 44.6, and 50.2, respectively (Table 5). This abnormality demonstrates that the tailings pond may comprise two distinct layers, an unchanged upper layer and the weathered layer in the deeper tailings.

## 4 Discussion

### 4.1 Carbonate weathering

We assume the carbonate weathering is likely occurring in the shallow layer. In this study, the CIA less than 55 situated in the shallow of the Wanniangou tailings pond (Drill-1  $\leq \sim 50$  m; Drill-2 and Drill-3  $\leq \sim 64$  m; Drill-4  $\leq \sim 90$  m; Table 3) reflects this layer has undergone minimal silicate weathering. Additionally, about 0.17 vol.% of calcite is present in the tailings waste (Table 2).

The dissolution of calcite is directly attributed to H<sup>+</sup> activity (Busenberg and Plummer 1982; Davis et al. 2007; Gautier et al. 1999), which is soluble in the tailings pond by comparison with silicate (Sun et al. 2022; Zhang et al. 2023). In the tailings profile, the carbon contents decrease from  $0.1 \pm 0.10$  wt.% to  $0.03 \pm 0.02$  wt.% in the shallow layer. Thus, the loss of inorganic carbon could be attributed to carbonate weathering.

In addition, sulfide oxidation is the dominant driver for chemical weathering in the tailings pond, as evidenced by the presence of minor pyrite pyrrhotite (FeS<sub>1-1.18</sub>) and pentlandite Fe(Ni,Fe)<sub>8</sub>S<sub>8</sub> (Pang et al. 2008; Tang 2017). The mine tailings contain a small proportion of sulfur in the tailings profile, ranging from 0.051 to 1.317 wt.%, and it declined in the drill cores ( $r: -0.81$ , Table 4). Meanwhile, Fig. 5 shows a negative correlation between SO<sub>3</sub> and CaO ( $r: -0.74$ ), revealing Ca<sup>2+</sup> alternatively leaching from carbonate (e.g., calcite) and silicate (plagioclase) minerals. Overall, the sulfide oxidation in the tailings pond can facilitate carbonate weathering.

### 4.2 Silicate weathering

Although carbonate is soluble in tailings pond, most ions migration is due to silicate weathering. Several

**Table 5** Coefficient variation of the upper and lower layers in the tailings profile

	Bulk CV	CV of upper layer					CV of lower layer				
		Drill-1	Drill-2	Drill-3	Drill-4	Mean	Drill-1	Drill-2	Drill-3	Drill-4	Mean
SiO <sub>2</sub>	9.1	7.1	4.3	11.2	4.6	6.8	7.0	14.6	9.2	3.4	8.5
MnO	10.6	9.7	7.3	8.6	6.4	8.0	6.2	11.7	8.4	2.0	7.1
P <sub>2</sub> O <sub>5</sub>	16.6	16.8	14.3	19.9	7.3	14.6	1.2	8.8	9.6	17.9	9.4
Fe <sub>2</sub> O <sub>3</sub>	17.3	14.1	10.4	20.9	10.0	13.8	7.1	17.7	9.4	3.9	9.5
BaO	19.1	11.6	7.0	12.2	7.2	9.5	16.6	15.2	12.5	24.0	17.1
TiO <sub>2</sub>	22.8	24.7	20.9	20.2	11.6	19.4	9.5	14.4	11.4	8.1	10.9
Al <sub>2</sub> O <sub>3</sub>	23.1	11.7	6.2	11.9	9.7	9.9	23.6	21.9	27.6	22.4	23.9
MgO	25.6	8.8	7.5	4.7	13.0	8.5	40.7	44.4	51.4	41.7	44.6
Na <sub>2</sub> O	26.0	14.5	7.0	16.0	15.5	13.2	45.5	43.8	45.0	13.8	37.0
CaO	29.2	5.7	9.3	11.9	11.6	9.6	48.7	49.0	59.6	43.6	50.2
K <sub>2</sub> O	30.0	26.2	18.0	30.1	23.8	24.5	22.3	36.3	15.0	34.3	27.0
V <sub>2</sub> O <sub>5</sub>	43.4	33.9	30.4	46.6	29.5	35.1	18.1	21.5	16.4	17.8	18.4
SO <sub>3</sub>	48.7	29.5	16.1	30.6	20.2	24.1	86.8	93.2	73.8	62.0	78.9
Cr <sub>2</sub> O <sub>3</sub>	52.7	44.9	40.9	55.4	33.6	43.7	14.7	15.7	34.7	28.6	23.4
Inorganic Carbon	79.8	37.6	59.1	32.9	46.3	44.0	44.6	84.8	78.7	77.5	71.4

The CV index could rise at very low concentration conditions (e.g., K<sub>2</sub>O and Cr<sub>2</sub>O<sub>3</sub>) and drop at high concentration conditions (e.g., SiO<sub>2</sub>)

observations support this claim: (1) abrupt changes in bulk elements, such as Al<sub>2</sub>O<sub>3</sub>, MgO, and CaO, were observed at depths  $\sim$  50 m (Drill-1),  $\sim$  64 m (Drill-2 and Drill-3), and  $\sim$  90 m (Drill-4), along with sudden changes in colour and texture. As seen in Fig. 2, the drill samples from the bottom are yellow, representing the transformation of ferrous iron to ferric iron. Meanwhile, the weathering degree increases with depths (CIA: Drill-1: 41–85, Drill-2: 43–94, Drill-3: 43–92, Drill-4: 44–80, Table 3), indicating intensive removal of alkali and alkaline earth elements (Liu et al. 2021; McLennan 1993). The increased weathering degree also reflects the degradation of feldspar and the formation of clays (Nesbitt and Young 1982).

(2) The Mg-silicate minerals are abundant in the tailings, such as chlorite (5.5 to 6 vol.%, mean 5.7 vol.%) and forsterite (4.2 to 6.3 vol.%, mean 5.2 vol.%, Table 2), while dolomite is rare. In the tailings profile, the SO<sub>3</sub> contents decreased along with MgO ( $r = 0.81$ , Fig. 5), probably suggesting Mg-silicate weathering. This is further supported by the degradation of mafic minerals (e.g., anorthite, diopside, and chrysotile) into chlorite, kaolinite, and montmorillonite assemblages (Fig. 3).

(3) Silicate weathering also leads to both dissolution and short-distance migration of SiO<sub>2</sub> in the tailings pond. The slight decline of SiO<sub>2</sub> in the tailings pond profile ( $r = -0.26$ , Table 4) and intensive decline in the bottom suggest that SiO<sub>2</sub> is in a declining tendency in the vertical direction. Likewise, the negative correlation between SO<sub>3</sub> and Al<sub>2</sub>O<sub>3</sub> ( $r = -0.745$ ) and Fe<sub>2</sub>O<sub>3</sub> ( $r = -0.232$ ) reveals the

H<sub>2</sub>SO<sub>4</sub> has accelerated such mafic minerals weathering (e.g., chlorite, forsterite, plagioclase, and pyroxene), and yield secondary minerals (e.g., montmorillonite and kaolinite, Fig. 3). In Table 2, the iron hydroxide and aluminium hydroxide are deposited in the lower tailings ponds. Therefore, this evidence assures that silicate weathering occurs in the deeper tailings pond.

The weathering rates of tailings can be accelerated by hydrated environments. As for mafic mine tailings, the dissolution of Mg<sup>2+</sup> and Ca<sup>2+</sup> in the tailings is consistent with the degradation of olivine and pyroxene. In Drill-1, the minerals reduction from 43.0 m to the bottom (53.0 m) infers the flow of water accelerates the chemical weathering in the tailings pond (Wilson et al. 2009). Likewise, other drill cores combine with the same feature in the aquifer zone (Fig. 4).

Meanwhile, runoff is another driver for silicate weathering (Dessert et al. 2003; Gaillardet et al. 1999). In flat terrain tailings ponds, stagnant water in decommissioning ponds is deemed an appropriate operation to limit the diffusion of oxygen and retard sulfide oxidation (Jackson and Parbhakar-Fox 2016). The Wanniangou tailings pond is a typical valley pond, with a designed height of 325 m and a starter dike designed with a permeable membrane for safety (Williams 2021). The structure of valley-type tailings ponds increases the fluidity of water, reduces the salinity of groundwater, and indirectly promotes the water-rock reaction. This leads to a more intensive chemical weathering process at the bottom of tailings ponds.

### 4.3 Contribution of carbonate and silicate weathering

#### 4.3.1 Upper layer

As mentioned above, we categorized the tailings profile into the upper and lower layers. The carbonate and silicate weathering proportion can be determined from Eq. 2 and Eq. 3 (Liu et al. 2008):

$$P_{carbonate} = \left\{ \frac{C}{X_{total}} \right\} \times 100 \quad (2)$$

$$P_{silicate} = \left\{ \frac{S}{X_{total}} \right\} \times 100 \quad (3)$$

where  $P$  represents the carbonate or silicate weathering proportion (%) in the tailings profile. The  $X_{total}$  represents the pristine CaO and MgO contents in the tailings, while the  $C$  and  $S$  represent the loss of carbonate and silicate, respectively. The loss of CaO and MgO in the tailings is due to either carbonate or silicate weathering. We suppose the CIA less than 55 as the fresh bulk MgO, CaO composition in the tailing, i.e. from 10.36 to 16.20 wt.% (mean 13.12 wt.%) and from 4.48 to 7.78 wt.% (mean 5.67 wt.%), respectively (Table 3), because the CIA range from 45 to 55 demonstrates minimal weathering (Liu et al. 2021; McLennan 1993). These values are comparable to those found in the Panxi V–Ti–Fe mine tailings (Tang 2017) and the regional basaltic rocks (Yang et al. 2017).

Besides, we use the bulk inorganic carbon composition in the Panxi V–Ti–Fe mine tailings pond to represent the initial carbon in this study ( $0.10 \pm 0.10$  wt.%, Appendix data). In the upper layer of the tailings pond, known as the carbonate-weathering layer, the average inorganic carbon decreased to  $0.035 \pm 0.020$  wt.%, that is 0.07 wt.% of net carbon loss. Based on Eq. 2, roughly 1.4% carbonate dissolution occurred in the upper layer.

#### 4.3.2 Lower layer

In the lower tailings pond, the inorganic carbon decreases from  $0.10 \pm 0.10$  wt.% to  $0.077 \pm 0.056$  wt.%, reveal slight carbonate dissolution. However, the MgO and CaO are intensively decreased to  $7.00 \pm 3.11$  wt.% and  $2.55 \pm 1.20$  wt.%, and a net loss of  $\sim 6.07$  wt.% and  $\sim 3.10$  wt.%, respectively. Based on Eqs. 2 and 3, the carbonate decomposition accounts for  $\sim 0.023$  wt.% (0.45%), and the silicate decomposition comprises 9.16 wt.% (48.4%). This corresponds to the V–Ti–Fe mine tailings ponds in the Panxi region, which experience both carbonates ( $\sim 5.1\%$ ) and silicates ( $\sim 79.2\%$ ) weathering (Zhang et al. 2023). Although carbonate weathering occurred throughout the entire tailings profile, its bulk

contribution was minor due to the lower level. In contrast, the silicate weathering led to greater ions dissolution in the tailings pond.

### 5 Conclusion

1. The Wanniangou tailings pond profile can be divided into the upper layer (carbonate weathering) and the lower layer (silicate weathering). This study reinforces that carbonate weathering occurs throughout the entire profile. Meanwhile, silicate weathering is the dominant chemical weathering process in the tailings pond, which is intensively influenced by sulfide oxidation and aquifers.
2. We monitored the transitions of carbonate to silicate weathering in the tailings profile. This rapid transition demonstrates that carbonate dissolution could mainly happen in the early stage of basalt weathering, and silicate weathering could become persistent over geological timescales.
3. The mineral dressing has exposed large quantities of fresh (ultra-)mafic hosted mine waste in the surficial environment. Our research draws an analogy to basalt weathering and supposes that carbonate weathering may preferentially occur in freshly exposed rock or the early stages. Likewise, human beings have been exposed to countless anthropogenic basalt interfaces on Earth, which may lead to a relatively higher proportion of carbonate weathering.

This study highlights the rapid transformation of carbonate weathering into silicate weathering in the Wanniangou V–Ti–Fe mine tailings pond. This switch demonstrates that the silicate weathering of basalt could be dominant in the geological time scale. We assume that the Al and Fe differentiation in chemical weathering could facilitate the enrichment of inert elements (e.g., Ti, Fe, Al) and potentially form valuable mineral deposits in the bottom of the valley-type tailings pond.

**Acknowledgements** This work was financially supported by Sichuan Science and Technology Program (No. 2023YFS0408).

**Author contributions** XZ: Validation, formal analysis, investigation, writing; YD: Funding acquisition; conceptualization, methodology, writing; LT: Review & editing, supervision; ZH: Review & editing; JY: Field investigation and sampling.

### Declarations

**Conflict of interest** The authors declare that they have no known competing financial interests or personal relationships that could have appeared to influence the work reported in this paper.

**Ethical approval** This material is the authors' own original work, which has not been previously published elsewhere. The paper is not currently being considered for publication elsewhere. The paper reflects the authors' own research and analysis in a truthful and complete manner. The paper properly credits the meaningful contributions of co-authors and co-researchers. The results are appropriately placed in the context of prior and existing research. All sources used are properly disclosed (correct citation). Literally copying of text must be indicated as such by using quotation marks and giving proper reference. All authors have been personally and actively involved in substantial work leading to the paper, and will take public responsibility for its content. The violation of the Ethical Statement rules may result in severe consequences.

## References

- Amiotte Suchet P, Probst JL, Ludwig W (2003) Worldwide distribution of continental rock lithology: Implications for the atmospheric/soil CO<sub>2</sub> uptake by continental weathering and alkalinity river transport to the oceans. *Global Biogeochem Cycles* 17(2):1038
- Bai X, Zhang S, Li C, Xiong L, Song F, Du C, Li M, Luo Q, Xue Y, Wang S (2023) A carbon neutrality capacity index for evaluating carbon sink contributions. *Environ Sci Ecotechnol* 15:100237
- Berndt ME, Allen DE, Seyfried WE (1996) Reduction of CO<sub>2</sub> during serpentinization of olivine at 300 °C and 500 bar. *Geology* 24(4):351–354
- Busenberg E, Plummer N (1982) The kinetics of dissolution of dolomite in CO<sub>2</sub>-H<sub>2</sub>O systems at 1.5 to 65 °C and 0 to 1 atm PCO<sub>2</sub>. *Am J Sci* 282:45–78
- Dai Q, Peng X, Yang Z, Zhao L (2017) Runoff and erosion processes on bare slopes in the karst rocky desertification area. *Catena* 152:218–226
- Dansgaard W (1964) Stable isotopes in precipitation. *Tellus* 16(4):436–468
- Das A, Krishnaswami S, Sarin MM, Pande K (2005) Chemical weathering in the Krishna Basin and Western Ghats of the Deccan Traps, India: Rates of basalt weathering and their controls. *Geochim Cosmochim Acta* 69(8):2067–2084
- Davis KJ, Nealson KH, Lütge A (2007) Calcite and dolomite dissolution rates in the context of microbe–mineral surface interactions. *Geobiology* 5(2):191–205
- Dessert C, Dupré B, François LM, Schott J, Gaillardet J, Chakrapani G, Bajpai S (2001) Erosion of Deccan traps determined by river geochemistry: impact on the global climate and the <sup>87</sup>Sr/<sup>86</sup>Sr ratio of seawater. *Earth Planet Sci Lett* 188(3–4):459–474
- Dessert C, Dupré B, Gaillardet J, François LM, Allègre CJ (2003) Basalt weathering laws and the impact of basalt weathering on the global carbon cycle. *Chem Geol* 202(3–4):257–273
- Gaillardet J, Dupré B, Louvat P, Allegre CJ (1999) Global silicate weathering and CO<sub>2</sub> consumption rates deduced from the chemistry of large rivers. *Chem Geol* 159(1–4):3–30
- Ganino C, Arndt NT (2009) Climate changes caused by degassing of sediments during the emplacement of large igneous provinces. *Geology* 37(4):323–326
- Ganino C, Arndt NT, Zhou M-F, Gaillard F, Chauvel C (2008) Interaction of magma with sedimentary wall rock and magnetite ore genesis in the Panzhihua mafic intrusion. SW China *Mineralium Deposita* 43(6):677–694
- Ganino C, Harris C, Arndt NT, Prevec SA, Howarth GH (2013) Assimilation of carbonate country rock by the parent magma of the Panzhihua Fe–Ti–V deposit (SW China): evidence from stable isotopes. *Geosci Front* 4(5):547–554
- Gautier M, Oelkers EH, Schott J (1999) An experimental study of dolomite dissolution rates as a function of pH from -0.5 to 5 and temperature from 25 to 80 °C. *Chem Geol* 157(1–2):13–26
- Georg RB, Reynolds BC, West AJ, Burton KW, Halliday AN (2007) Silicon isotope variations accompanying basalt weathering in Iceland. *Earth Planet Sci Lett* 261(3–4):476–490
- Hangx SJT, Spiers CJ (2009) Reaction of plagioclase feldspars with CO<sub>2</sub> under hydrothermal conditions. *Chem Geol* 265:88–98
- Hill IG, Worden RH, Meighan IG (2000) Yttrium: the immobility-mobility transition during basaltic weathering. *Geology* 28(10):923–926
- Jackson LM, Parbhakar-Fox A (2016) Mineralogical and geochemical characterization of the Old Tailings Dam, Australia: evaluating the effectiveness of a water cover for long-term AMD control. *Appl Geochem* 68:64–78
- Jacobson AD, Grace Andrews M, Lehn GO, Holmden C (2015) Silicate versus carbonate weathering in Iceland: new insights from Ca isotopes. *Earth Planet Sci Lett* 416:132–142
- Johnson NM, Driscoll CT, Eaton JS, Likens GE, McDowell WH (1981) ‘Acid rain’, dissolved aluminum and chemical weathering at the Hubbard Brook experimental forest, New Hampshire. *Geochim Cosmochim Acta* 45(9):1421–1437
- Li J, Zhang B, Yang M, Lin H (2021) Bioleaching of vanadium by Acidithiobacillus ferrooxidans from vanadium-bearing resources: performance and mechanisms. *J Hazard Mater* 416:125843
- Li C, Bai X, Tan Q, Luo G, Wu L, Chen F, Xi H, Luo X, Ran C, Chen H (2022) High-resolution mapping of the global silicate weathering carbon sink and its long-term changes. *Glob Change Biol* 28(14):4377–4394
- Liu C-Q, Jiang Y-K, Tao F-X, Lang Y-C, Li S-L (2008) Chemical weathering of carbonate rocks by sulfuric acid and the carbon cycling in Southwest China (in Chinese). *Acta Geochimica* 37(4):404–414
- Liu J-C, He H-P, Michalski J, Cuadros J, Yao Y-Z, Tan W, Qin X-R, Li S-Y, Wei G-J (2021) Reflectance spectroscopy applied to clay mineralogy and alteration intensity of a thick basaltic weathering sequence in Hainan Island. *South China Appl Clay Sci* 201:105923
- McLennan SM (1993) Weathering and global denudation. *J Geol* 101(2):295–303
- Meyer NA, Vögeli JU, Becker M, Broadhurst JL, Reid DL, Franzidis JP (2014) Mineral carbonation of PGM mine tailings for CO<sub>2</sub> storage in South Africa: A case study. *Miner Eng* 59:45–51
- Nelson CJ, Jacobson AD, Weisenberger TB (2022) Controls on riverine calcium isotope ratios during basalt weathering in the Skagafjörður watershed, Iceland. *Geochim Cosmochim Acta* 333:216–241
- Nesbitt H, Young G (1982) Early Proterozoic climates and plate motions inferred from major element chemistry of lutites. *Nature* 299(5885):715–717
- Nishimura A, Tabuchi Y, Kikuchi M, Masuda R, Goto K, Iijima T (2016) The amount of fluid given during surgery that leaks into the interstitium correlates with infused fluid volume and varies widely between patients. *Anesth Analg* 123(4):925–932
- Pang K-N, Zhou M-F, Lindsley D, Zhao D, Malpas J (2008) Origin of Fe–Ti oxide ores in mafic intrusions: Evidence from the Panzhihua intrusion, SW China. *J Petrol* 49(2):295–313
- Rey NJ, Demers I, Bussière B, Mbonimpa M, Lortie S (2016) Field experiments to test the elevated water table concept combined with a desulfurized tailings cover layer. *Geo-Chicago* pp 289–298
- Schober P, Boer C, Schwarte LA (2018) Correlation coefficients: Appropriate use and interpretation. *Anesth Analg* 126(5):1763–1768

- Schwartzman DW, Volk T (1989) Biotic enhancement of weathering and the habitability of Earth. *Nature* 340(6233):457–460
- Shi H, Tang L, Chen Y, Shi M (2020a) Pb, Zn leaching law in vanadium - titanium magnetite tailings (In Chinese). *Environ Sci and Manag* 45(11):68–73
- Shi M, Tang L, Chen Y, Shi H-B, Zhou S-F (2020b) Study on Mn, Fe leaching law from vanadium-titanium magnetite ore tailings (In Chinese). *Sichuan Environ* 39(4):16–22
- Sun L, Werner T, Yang F, Xu W, Tang L (2022) CO<sub>2</sub> fluxes in the chemical weathering of carbonate-hosted tailings ponds, Panxi valley, Sichuan province. *China Environ Earth Sci* 81(15):392
- Tang L (2017) Inverstigation on the mineralization of tailings with CO<sub>2</sub> in the atmosphere (In Chinese). Sichuan University, Chengdu, China, pp 1–160
- Tang L, Werner TT (2023) Global mining footprint mapped from high-resolution satellite imagery. *Commun Earth & Environ* 4(1):134
- Tang L, Liu X, Wang X, Liu S, Deng H (2020) Statistical analysis of tailings ponds in China. *J Geochem Explor* 216:106579
- Tang L, Werner TT, Xie H, Yang J, Shi Z (2021) A global-scale spatial assessment and geodatabase of mine areas. *Global Planet Change* 204:103578
- Taylor R (1990) Interpretation of the correlation coefficient: a basic review. *J Diagnostic Med Sonogr* 6(1):35–39
- Taylor AS, Lasaga AC (1999) The role of basalt weathering in the Sr isotope budget of the oceans. *Chem Geol* 161(1–3):199–214
- Velbel MA, Barker WW (2008) Pyroxene weathering to smectite: conventional and cryo-field emission scanning electron microscopy, Koua Bocca ultramafic complex. *Ivory Coast Clays and Clay Minerals* 56(1):112–127
- Vogeli J, Reid DL, Becker M, Broadhurst J, Franzidis J-P (2011) Investigation of the potential for mineral carbonation of PGM tailings in South Africa. *Miner Eng* 24(12):1348–1356
- Williams DJ (2021) Lessons from tailings dam failures - where to go from here? *Minerals* 11(8):853
- Wilson SA, Raudsepp M, Dipple GM (2009) Quantifying carbon fixation in trace minerals from processed kimberlite: a comparative study of quantitative methods using X-ray powder diffraction data with applications to the Diavik Diamond Mine, Northwest Territories. *Canada Appl Geochem* 24(12):2312–2331
- Xiao B, Bai X, Zhao C, Tan Q, Li Y, Luo G, Wu L, Chen F, Li C, Ran C (2023) Responses of carbon and water use efficiencies to climate and land use changes in China's karst areas. *J Hydrol* 617:128968
- Xing C, Wang CY, Zhang M (2012) Volatile and CHO isotopic compositions of giant Fe-Ti-V oxide deposits in the Panxi region and their implications for the sources of volatiles and the origin of Fe-Ti oxide ores. *Sci China Earth Sci* 55(11):1782–1795
- Xiong L, Bai X, Zhao C, Li Y, Tan Q, Luo G, Wu L, Chen F, Li C, Ran C, Xi H, Luo X, Chen H, Zhang S, Liu M, Gong S, Xiao B, Du C, Song F (2022) High-resolution data sets for global carbonate and silicate rock weathering carbon sinks and their change trends. *Earth's Future* 10(8):1–18
- Xu L, Tang L, Zhang X, Hou Z, Haris M, Luo J, Yang Y (2022) Mine waste water self-purification (arsenic) in neutral hydrogeochemical ecosystem: a case study from V-Ti-Fe mine tailings. *Geochemistry* 83(2):125947
- Yamada I, Shoji S (1987) Weathering of titanomagnetite in a recent rhyolitic ash in Miyagi Prefecture Japan. *Soil Sci and Plant Nutrit* 33(3):493–499
- Yang H-Y (1987) Stability of ilmenite and titanomagnetite in the presence of carbon dioxide - a thermodynamic evaluation. *Contrib Miner Petrol* 95(2):202–206
- Yang Y-J, Zhu W-G, Bai Z-J, Zhong H, Ye X-T, Fan H-P (2017) Petrogenesis and tectonic implications of the Neoproterozoic Datian mafic-ultramafic dykes in the Panzhihua area, western Yangtze Block, SW China. *Int J Earth Sci* 106(1):185–213
- Zhang X, Gou L-F, Tang L, Liu S, Werner TT, Mudbhakal A, Jiang F, Deng Y 2023. Transitions of CO<sub>2</sub> degassing to sequestration during chemical weathering of (ultra-)mafic mine tailings. *Journal of Geochemical Exploration*, Under review pp 1–22.
- Zhou M, Robinson PT, Lesher GM, Keays RR, Zhang C, Malpsa J (2005) Geochemistry, petrogenesis and metallogenesis of the panzhihua gabbroic layered intrusion and associated Fe-Ti-V oxide deposits, Sichuan Province, SW China. *J Petrol* 46(11):2253–2280
- Zielke-Olivier J, Vermeulen P (2019) A geochemical weathering profile of a fine ash tailings dam and its impact on the underlying aquifers. *J Environ Manage* 242:162–170

Springer Nature or its licensor (e.g. a society or other partner) holds exclusive rights to this article under a publishing agreement with the author(s) or other rightholder(s); author self-archiving of the accepted manuscript version of this article is solely governed by the terms of such publishing agreement and applicable law.